Laser Photonics Rev. **7,** No. 6, 1079–1087 (2013) / **DOI** 10.1002/lpor.201300111

LASER & PHOTONICS REVIEWS

Abstract An effective method is presented for enhancing the outcoupling efficiency of translucent/bi-directional organic light-emitting diodes (TL/BD-OLEDs) with a bottom indium tin oxide (ITO) anode and a top cathode comprised of a thin Ag layer covered with an organic capping layer. Upon insertion of a nanoparticle (NP)-based scattering layer (NPSL) between the substrate and the ITO anode, the TL/BD-OLEDs exhibit significantly enhanced external quantum efficiency (EQE) in both emission directions. Furthermore, the NPSL improves the color stability of the TL/BD-OLEDs over a wide range of viewing angles. Simulations based on geometrical and statistical optics are performed to elucidate the mechanism by which the efficiency is enhanced and to establish strategies for further optimization. Simulations performed on the scattering layers with varying NP volume percentage reveal that the bottom-side emission is governed by competition between waveguide-mode extraction and backward scattering by NPs in the film, while the top-side emission is largely dominated by the latter. Optimized bi-directional OLEDs achieve a 1.64-fold enhanced EQE compared to reference devices without NPSL.

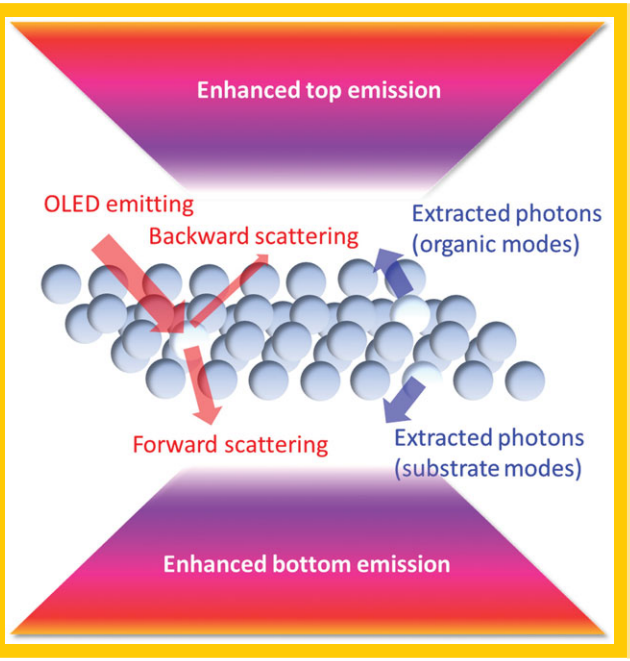

ORIGINAL PAPER

Bi-directional organic light-emitting diodes with nanoparticle-enhanced light outcoupling

Hong-Wei Chang[1,2,], Jonghee Lee[1,3,**], Tae-Wook Koh[4], Simone Hofmann[1], Björn Lüssem[1], Seunghyup Yoo[4,*], Chung-Chih Wu[2,*], Karl Leo[1,*], and Malte C. Gather[1,*,††]**

1. Introduction

Organic light-emitting diodes (OLEDs) exhibiting translucent properties and bi-directional emission are promising for use in next-generation display and lighting applications [1–3]. Translucent/bi-directional OLEDs (TL/BD-OLEDs) emit light through both bottom and top contact and offer a high degree of optical transparency. As in conventional OLEDs, device efficiency is also a key performance parameter in TL/BD-OLEDs; thus, many studies have attempted to improve efficiency. For example, a dielectric capping layer (consisting of, e.g., ZnSe, WO_3, ZnS, or an organic material) [4–6] is introduced on top of a thin metal film to adjust the transmittance/reflectance of the top electrodes, thus increasing the external quantum efficiency (EQE) for one or both emission directions. Double-layer cathode structures of Mg/Ag, Ca/Ag, or Ba/Ag [7–9] are often used to exploit the low-absorption properties of Ag while ensuring efficient electron injection. Oxide/metal/oxide (OMO)-based top transparent electrodes such as ITO/Ag/ITO have also proven useful [10].

The outcoupling efficiency (η_{out}) is regarded as a key factor limiting the efficiency of OLEDs [11–13]. The total EQE of an OLED is given by the product of the internal quantum efficiency (IQE) and the outcoupling efficiency η_{out}. While IQE values approaching 100% have been reported in well-designed phosphorescent OLEDs [14], the η_{out} values are typically below 20–30% [15] unless the emission layer contains emitter molecules with transition dipoles predominantly oriented parallel to a substrate [16].

[1] Institut für Angewandte Photophysik, Technische Universität Dresden, George-Bähr-Straße 1, 01062 Dresden, Germany
[2] Graduate Institute of Electronics Engineering, Graduate Institute of Photonics and Optoelectronics and Department of Electrical Engineering, National Taiwan University, Taipei 106, Taiwan
[3] OLED Research Team, Electronics and Telecommunications Research Institute (ETRI), Daejeon 305–700, South Korea
[4] Department of Electrical Engineering, Korea Advanced Institute of Science and Technology (KAIST), 373-1 Guseong-dong, Daejeon 305–701, South Korea
[**] Authors contributed equally to this work.
[††] Present address: SUPA, School of Physics and Astronomy, University of St Andrews, St Andrews KY16 9SS, UK
[*] Corresponding authors: e-mail: syoo.ee@kaist.edu; chungwu@cc.ee.ntu.edu.tw; karl.leo@iapp.de; malte.gather@iapp.de

To overcome this "outcoupling bottleneck," several novel device architectures have been proposed and tested, though most research has focused on conventional OLEDs. While the concepts behind these architectures may also apply to TL/BD-OLEDs, the details of their working mechanisms could differ significantly due to the specific optical structure of TL/BD-OLEDs. For example, an outcoupling architecture that relies heavily on light reflected from the top electrode would not work effectively in a TL/BD-OLED due to the lack of substantial reflection from the top electrode in these devices. In some cases, an outcoupling structure may provide efficient emission in one direction, but not in the other. Hence, for each structure, one must ensure compatibility with TL/BD-OLEDs.

In this work, we explore the feasibility of improving light extraction in TL/BD-OLEDs using nanoparticle-based scattering layer (NPSL). Previous studies have shown that NPSL is highly effective for light extraction in white OLEDs and can improve the incoupling of light in organic solar cells [17]. By carefully monitoring the bi-directional optical characteristics of the NPSL, their effect on the emission in each direction and on the EQE and angular/spectral emission characteristics of the devices are studied in detail. We then use optical simulations to analyze the experimental results, to gain insight into the underlying mechanisms, and to develop strategies for further optimization.

2. Experimental

2.1. NPSL formation

The NPSL investigated here is comprised of a transparent polymer into which TiO_2 particles of high refractive index are embedded. A total of 0.6 g TiO_2 NPs (mean diameter 240 nm, Centron Biochemistry Technology Co., Ltd) are dispersed in 4 mL of propylene glycol-monomethyl-ether acetate (PGMEA) solution containing the optical polymer host matrix (EOC130, Everlight Chemical). ZrO_2 particles (mean diameter, 100 μm) are added to the mixture as milling objects. A homogenous dispersion is achieved by physical vibration, stirring, and milling the mixture for 24 h. The dispersion is subsequently filtered (pore size, 5 μm) to remove the milling particles. The NPSL is fabricated by spin-coating (1,000 rpm, 40 s) onto $2'' \times 2''$ substrates and are subsequently heat-cured (130°C, 10 min) to remove any residual solvent and to promote the formation of a smooth film. The solid content of the original PGMEA polymer solution is 30%, yielding a TiO_2 particle concentration (density, ~4.24 g/mL) of approximately 12 ± 4 vol% in the final film, which corresponds to a particle density of 20 μm^{-3}.

2.2. Device fabrication

We use red phosphorescent transparent/bi-directional OLEDs with a p–i–n doped structure and an organic capping layer in this study as illustrated in Figs. 1(a) and (b). The detailed structure of the stack is: indium tin oxide (ITO, 100 nm)/p-layer/N-N′-di(naphthalene-1-yl)N, N′-diphenyl-benzidine (NPB, 10 nm)/emission layer (20 nm)/bis(2-,ethyl-8-quinolinolato)-4-(phenyl-pheno-lato) aluminum-(III) ($BAlq_2$, 10 nm)/n-layer/Ag (15 nm)/NPB (capping layer, 140 nm). The p-layer comprises of 60-nm-thick films of N,N,N,N′-tetrakis(4-methoxyphenyl)-benzidine (MeO-TPD) doped with 4 wt% of Novaled dopant p-type 2 (NDP-2, Novaled AG). The n-layer comprises of 60 nm of cesium-doped 4,7-diphenyl–1,10-phenanthroline (BPhen) with a conductivity comparable to that of the p-side. The 20-nm-thick red EML consists of NPB doped with 10% of the triplet red

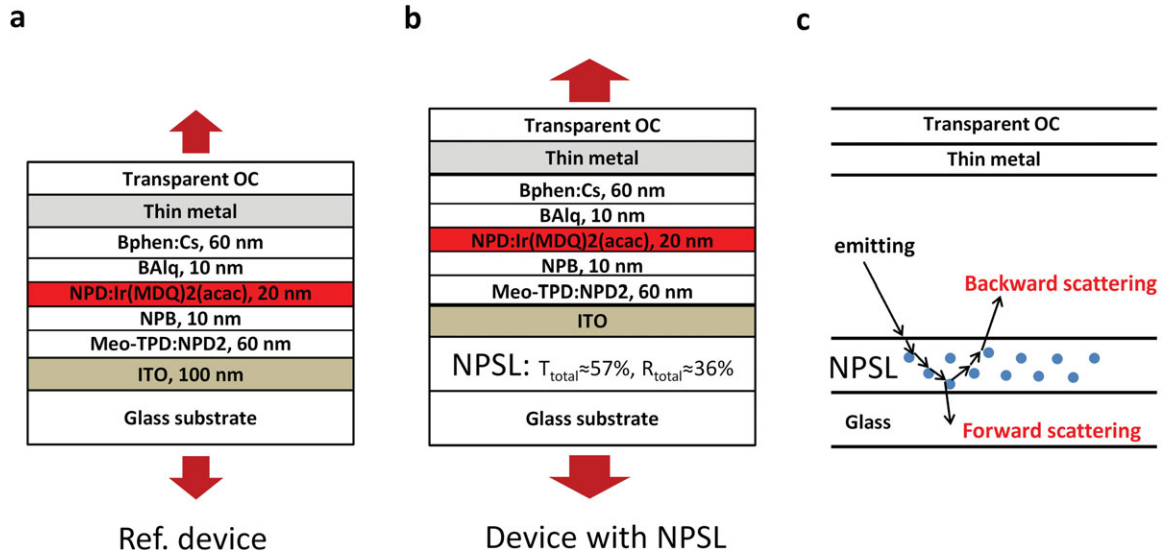

Figure 1 Schematic illustrations of NPSL applied to bi-directional OLEDs. a) Structure of a conventional device. b) Structure of a device with embedded NPSL. c) Schematic of the bimodal extraction of photons via forward and backward scattering.

emitter iridium (III)bis [2-methyldibenzo-(f,h) quinoxaline](acetylacetonate) ($Ir(MDQ)_2(acac)$). ITO anodes are deposited on NPSL by RF magnetron sputtering through a contact metal mask. Reference devices are fabricated on ITO coated glass substrates. The other layers of the stack are deposited onto the ITO-anodes via thermal evaporation in an ultra-high-vacuum chamber (Kurt J. Lesker Co.) at a base pressure of approximately 10^{-8} mbar.

2.3. OLED characterization

OLEDs are characterized by recording current-voltage characteristics as well as electroluminescence spectra in forward direction and as a function of angle. Current-voltage characteristics of the devices are recorded with a Keithley 2400 source measuring unit. Simultaneously spectra are collected with an Instrument Systems GmbH CAS140 spectrometer and the device luminance in the forward direction is measured with a calibrated silicon photodiode (Hamamatsu). The angular emission characteristics of the OLED are measured with a spectrogoniometer setup to estimate the external quantum efficiency and power efficacy.

2.4. Simulation

To better understand the mechanism behind the enhanced light extraction in NPSL-based devices, we use optical simulation software. This enables us to calculate the haze of the NPSL alone and to model the emission from bi-directional OLEDs comprising NPSLs. Both calculations are based on the geometrical/statistical optics software (LightTools™, Optical Research Associates). All calculations are performed for a wavelength of 610 nm.

(a) Haze calculation model: A point source is placed in the ambient air and is set to emit a collimated beam (angle $< 1^\circ$) normal to the NPSL. A hemispherical absorber is placed on the backside to absorb any scattered light and eliminate unwanted backward reflection in the NPSL. A far-field receiver collects the total transmitted power. An additional small planar receiver is placed behind the substrate to collect specular transmission (collection angle 2.5°).

(b) Bi-directional OLED model: A 2-μm-thick NPSL (n = 1.52 for the host matrix, n = 2.2 for the scattering particles) is placed on top of a 700-μm-thick glass substrate (n = 1.52). A 100-nm thick ITO layer (n = 1.95) and a 160-nm thick organic layer (n = 1.75) are placed on top, and the top surface of the organic layer is set to have T/A/R values as indicated in the main text. All vertical surfaces are set to be absorbing to eliminate unwanted side emissions. An isotropic point source with an emitting power of 100 lm is immersed in the organic layer, and two planar receivers are placed on the top/bottom sides of the bi-directional OLEDs to collect the power emitted into each direction.

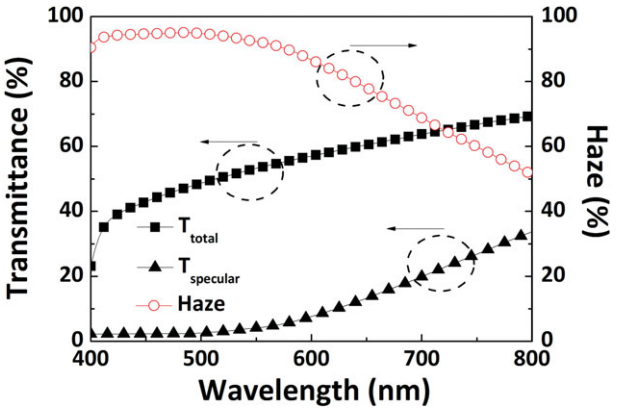

Figure 2 Spectra of total transmittance (T_{total}, black square ■), specular transmittance ($T_{specular}$, black triangle ▲) and haze (red circle ○) of NPSL sample. T_{total} is measured with an integrating sphere, and $T_{specular}$ refers to the direct photon flux through the sample.

3. Results and discussion

Figures 1(a) and (b) provide schematic structures of a conventional TL/BD-OLED and the proposed device with the NPSL, respectively. Figure 1(c) presents sample ray diagrams pertaining to the operation of a TL/BD-OLED with the NPSL. When light interacts with the particles, both forward scattering and backward scattering occur. By disturbing total internal reflection at the glass/ITO interface, the forward scattering effect is expected to lead to extraction of photons (toward the bottom side) that would otherwise be confined within the OLED stack [18–20]. The backward scattering effect can be subtle and may involve several sequential steps. If a photon is initially scattered backward towards the top electrode at an incident angle that is larger than the critical angle (θ_c) between the organic layers and the surrounding air, the photon will not be extracted directly but will rather be reflected toward the scattering layer. Subsequently, the photon may either be extracted in the bottom direction or reflected back toward the top direction at a different angle. This process can be repeated several times until the photon is either extracted or lost as residual internal absorption. However, if a photon is initially scattered backward and the incident angle is smaller than θ_c, it will either be emitted through the top electrode or it will be reflected at the top electrode (with the probability of each process depending on the transmittance (T_{top}) and reflectance (R_{top}) of the top electrode) [21].

Figure 2 presents the optical characteristics of the NPSL investigated in this work, including their total transmittance (black squares, T_{total}), as measured by an integrating sphere module (JASCO, UV570 spectrophotometer), and their specular transmittance (black triangles, $T_{specular}$).

Table 1 Optical characteristics* and roughness of the NPSL.

T_{total} (%)	$T_{diffuse}$ (%)	$T_{specular}$ (%)	R_{total} (%)	Haze (%)	Ra (nm)
57.7	49.1	8.6	36.8	85.0	3.6

*Measured at the wavelength of 610 nm.

Based on these data, one can determine the haze value, which quantifies the degree of scattering in the films. At a wavelength (λ) of 610 nm, which corresponds to the peak emission wavelength of the red phosphorescent emitter used in this study, $T_{diffuse} = T_{total} - T_{specular} = 49.1\%$ and haze $= T_{diffuse}/T_{total} = 85\%$. These numbers indicate that the use of NPSL results in a substantial scattering effect. The value of R_{total} is measured at 36.9%, indicating that the backward scattering is also significant in the studied films. A high degree of scattering is observed across the entire visible spectrum, which has proven beneficial for enhancing spectrally neutral outcoupling [17].

Obtaining NPSLs with sufficient surface flatness is challenging but critical to ensuring low leakage currents during electrical operation. Thermal curing during NPSL fabrication is found to improve surface flatness. For the tested films, a relatively low surface roughness (RMS $<$ 4 nm, 5 $\times$ 5 μm^2) is achieved. In Table 1, we summarize the values for T_{total}, $T_{specular}$, R_{total}, haze, and surface roughness of the NPSL.

Figures 3(a) and (b) show the current density (J)–voltage (V)–luminance (L) characteristics of the studied OLEDs as measured in the bottom and top directions, respectively. The J–V curves and the electroluminescence (EL) onset voltages ($\sim$2.5 V) of the NPSL-based OLEDs are nearly identical to those of the reference TL/BD OLEDs, indicating that the insertion of the NPSL does not alter the electrical characteristics of the OLEDs. Their influence may thus be largely considered a result of optical phenomena. In contrast to the J–V curves that remain virtually unchanged, a significant enhancement in luminance is observed. At a driving current of 1 mA (= 15 mA/cm^2), the device containing the NPSL reaches a luminance of 2597 cd/m^2 and 607 cd/m^2 for the bottom and the top-side emission, respectively. These values correspond to a 1.93- and 2.57-fold enhancement with respect to the luminance obtained of the reference device. This corresponds to an increase in total luminance by a factor of 2.03.

Not only the luminance but also the power efficiency (PE) and EQE, which take into account the emission characteristics across the all emission angles, exhibit a significant improvement. As shown in Figs. 4(a)–(d) insertion of the NPSL also enhances PE and EQE in both emission directions: at a driving current of 1 mA the PE increases by 1.56-fold for the bottom-side emission and 2.17-fold for the top-side emission. Likewise, the EQE increases 1.53-fold for the bottom-side emission and 2.12-fold for the top-side emission. Because the relative enhancement is larger for the top-side than for the bottom-side emission, the ratio of bottom-to-top emission becomes more balanced when inserting the NPSL: The ratio changes from 4.71 (PE) and 4.78 (EQE) in the reference device to 3.40 (PE) and 3.46 (EQE) in the NPSL-based OLED (see Table 2 for a performance comparison summary).

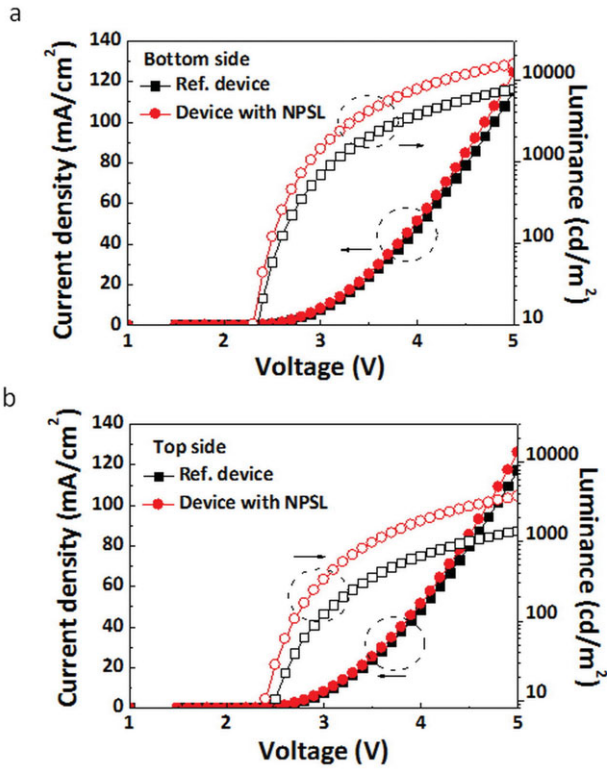

Figure 3 *J–V–L* characteristics of a bi-directional red OLED with and without NPSL. a) Characteristics for bottom-side emission and b) characteristics for top-side emission for a reference device (black squares ■) and for the devices with NPSL (red circles •).

Figure 5 indicates that an enhancement in luminance is present across the entire spectral range and that the overall shape and peak wavelength of the EL spectra are only slightly altered by the insertion of the NPSL. Furthermore, Figs. 6(a) and (b) indicate that the CIE 1931 xy color coordinates become more stable with respect to the viewing angle upon insertion of the NPSL. The maximum color difference can be estimated by the Euclidean distance ΔE_{xy} between the CIE color points at 0° and 70° [22]. For bottom emission, the ΔE_{xy} values are 0.017 and 0.001 for the reference device and for the device with the NPSL, respectively. For top emission, the ΔE_{xy} values are 0.017 and 0.007. This chromaticity-stabilizing effect is attributed to the fact that the NPSL randomizes the emission angles. This property is highly advantageous and differentiates the NPSL from several other outcoupling approaches, which suffer from severe angular or spectral dependence [23].

The randomizing effect of the NPSL is also apparent in the change of radiance with viewing angle. As shown in Figs. 7(a) and (b), the normalized radiance given as a function of the viewing angle becomes more Lambertian upon insertion of the NPSL. For bottom-side

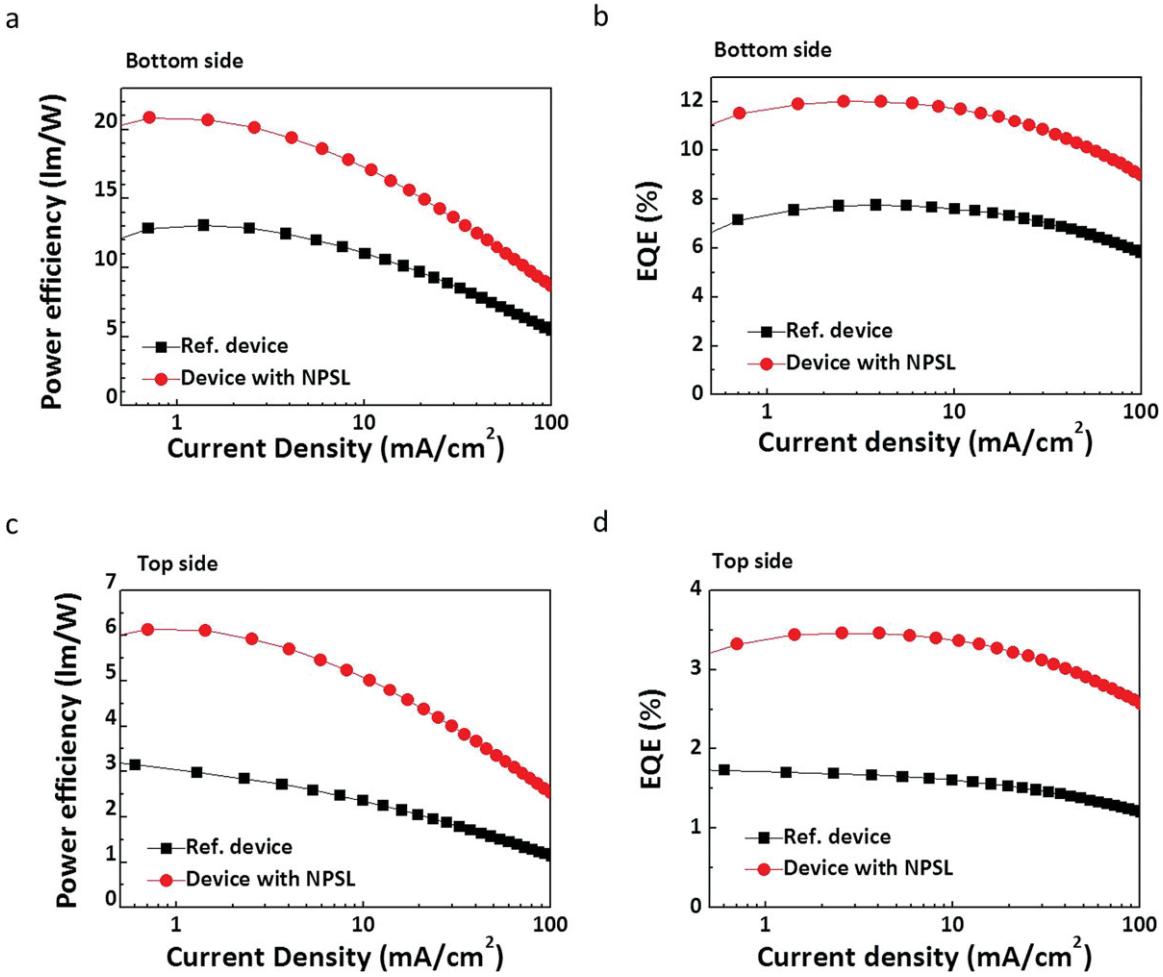

Figure 4 Power efficiency (PE) and external quantum efficiency (EQE) versus current density in the TL/BD-OLEDs: PE (a/c) and EQE (b/d) for the bottom-side/top-side emission. Data for the reference device are denoted by black squares ■, and those for the devices containing the NPSL are shown by red circles ●.

Table 2 Summary of the performance of TL/BD-OLEDs*.

@ 1 mA (15 mA/cm^2)	Emitted direction	ΔE_{xy}	Brightness (cd/m^2)	EQE (%)	X EQE	Total EQE (%)	PE (lm/W)	X PE	Total PE (lm/W)
Control Device	Bottom	0.017	1340.4	7.46	–	9.02%	10.24	–	12.41
	Top	0.017	236.1	1.56	–		2.17	–	
Device with NPSL	Bottom	0.001	2596.5	11.45	X 1.53	14.75% (X 1.64)	15.99	X 1.56	20.69 (X 1.67)
	Top	0.007	607.2	3.30	X 2.12		4.70	X 2.17	

*Data measured and calculated for a current density of 15mA/cm^2, including the enhancement in EQE and PE for the bottom, top, and total emission, and the color stability expressed as the Euclidean distance (ΔE_{xy}) for emission under 0° and 70°.

emission, the device containing the NPSL emits light almost as a perfect Lambertian emitter i.e. the luminance remains nearly constant regardless of the viewing angle. For top-side emission, both the reference devices and the device with NPSL show significant departure from the Lambertian characteristics. Nevertheless, the angular emission characteristics of the device containing the NPSL more closely resemble a Lambertian distribution than the emission of the reference device.

To better understand the mechanism behind the enhanced light extraction in NPSL-based devices and, in particular, to model the specific emission behavior in top and

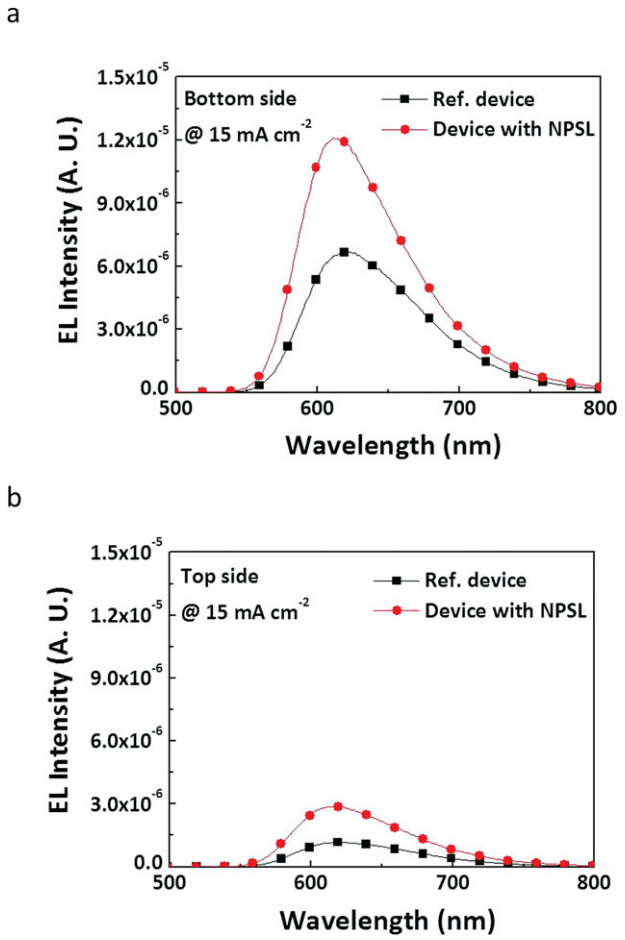

Figure 5 EL intensity versus wavelength measured at a driving current of 15 mA cm^{-2} in bi-directional OLEDs. a) EL intensity of the bottom-side emission and b) EL intensity of the top-side emission for a reference device (black line ■) and device with NPSL (red line •).

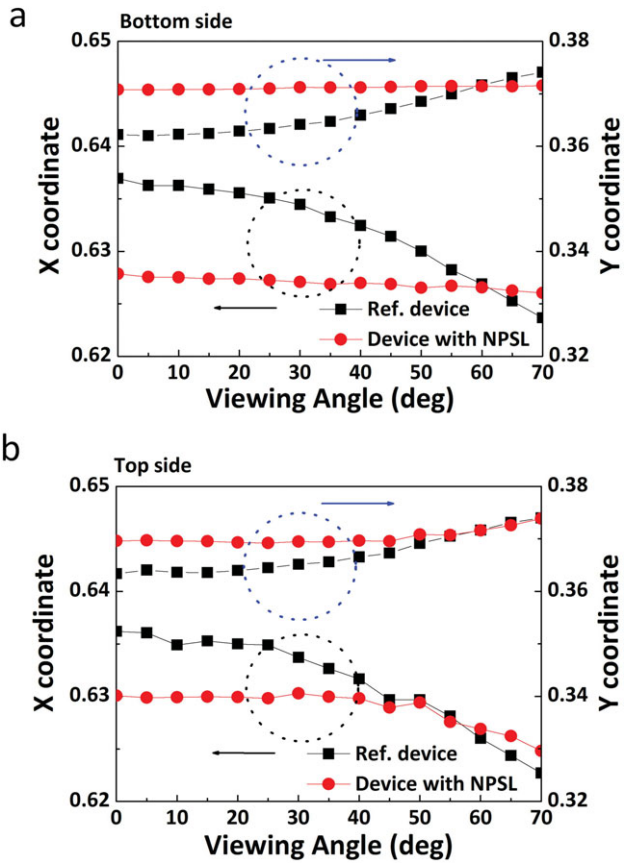

Figure 6 Variation in the CIE coordinates over viewing angle with respect to a) bottom-side emission and b) top-side emission for both a reference device (black squares ■) and device with NPSL (red circles •).

the bottom direction, we use optical simulation software. In the following, two 3D models are discussed: The first explores the haze phenomenon of the NPSL, quantifying the haze value according to the ASTM D1003–11 standard. The second model explores the effect of the NPSL on the light extraction efficiency of TL/BD-OLEDs. In both cases, the following model parameters are employed: 1) the volume percentage (vol%) of the scattering particles in the host medium and 2) the size (radius) distribution of the NPs (σ_R, standard deviation of size, assuming a Gaussian distribution with a mean particle radius of 120 nm). We firstly calculate the specular transmittance ($T_{spec}^{(cal)}$) and the total transmittance ($T_{total}^{(cal)}$) of the NPSL at a fixed wavelength of 610 nm for varying concentration and σ_R of NPs (Figs. 8(a) and (b)). At the nominal particle concentration in our samples (12 ± 4 vol%) $T_{spec}^{(cal)}$ and $T_{total}^{(cal)}$ are in between 27.1% to 8.0% and 69.7% to 59.4%, respectively, depending on the size spread σ_R. These values are somewhat higher than the experimentally obtained values ($T_{spec}^{(exp)} = 8.63\%$; $T_{total}^{(exp)} = 57.7\%$). We believe that this difference is in part due to the fact that the actual particle concentration in our samples is higher than the nominal 12 vol%.

In the second model, the NPSL is incorporated into a simplified TL/BD OLED structure consisting of a glass substrate (n = 1.52)/NPSL (optional)/ITO (n = 2.0)/organic layer stack (n = 1.75)/top electrode. Because modeling the Ag/NPB top electrode with the software used is not straightforward, this electrode is not directly included in the device structure for modeling; instead, the top surface of the organic layer is constrained to have a T/A/R value of 25%/17%/58% in the normal direction, which are the values expected for the Ag/NPB combinations used in this work. The calculation is then performed using an isotropic, monochromatic (λ = 610 nm) point source embedded in the organic layer as emitting site. When the NPSL is not included in the model, the outcoupling efficiencies (η_{out}) are calculated as 2.5% and 11.5% for the top and bottom emission directions, respectively, corresponding to a top/bottom ratio of 1:4.6, which is close to the top/bottom ratio of EQE (1:4.8) obtained experimentally for the reference

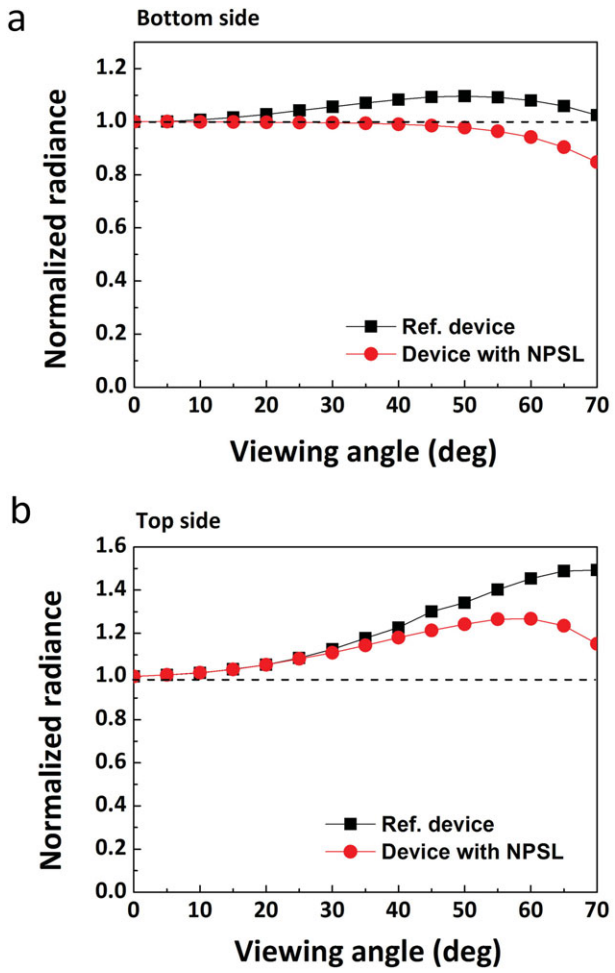

Figure 7 Variation in the normalized radiance over different viewing angles with respect to a) bottom-side emission and b) top-side emission for the reference devices (black squares ■) and for devices containing NPSL (red circles •).

device. Upon inclusion of the NPSL, with the same model parameters as used to model the haze characteristics, the η_{out} values are estimated at 6.6% and 21.4% for the top and bottom emissions respectively. These values correspond to an EQE top/bottom ratio of 1:3.2 and relative enhancement factors of 2.64 (top) and 1.86 (bottom). Although the calculated values differ slightly from the experimentally obtained EQE top/bottom ratio of 1:3.5, the enhancement factors of 2.1 (top) and 1.5 (bottom) are in a relatively good agreement given the simplifications used in the model such as the assumption of monochromic emitters. The trends are clearly consistent with the experimental observations: the top/bottom ratio tends toward a more balanced emission, and the relative enhancement factor is larger for the top-emitting direction than for the bottom-emitting direction.

Simulation results obtained for varying particle concentration at a fixed σ_R of 10 nm further elucidate the properties observed in our TL/BD-OLEDs. Figures 8(c) and (d) show the outcoupling efficiency, η_{out}, calculated for bottom and top emission versus particle concentration in vol%. For the bottom-side emission, η_{out} first increases with increasing NP concentration, but begins to decrease after the concentration exceeds approximately 7 vol%. In contrast, for the top-side emission, η_{out} continues to grow as the particle concentration increases. This means that the enhancement of the top-side emission is caused by backward reflection/scattering from the NPSL, while the enhancement of the bottom-side emission primarily originates from the disruption of waveguide modes. The simulation results indicate that the backward reflection/scattering increases with particle concentration, in correlation with the growth in η_{out} for top-side emission. For the bottom-side emission, the waveguide-mode extraction due to (forward) scattering at the NPs competes with the backward scattering/reflection, which in fact reduces outcoupling to the bottom-side. The effect of backward scattering becomes dominant as the NP density increases beyond a concentration of about 7 vol%. Therefore, with regard to outcoupling in bottom direction there is an optimum concentration of particles in the NPSL.

4. Conclusions

NPSLs are introduced as an effective method for enhancing the outcoupling efficiency of TL/BD-OLEDs comprised of an ITO-bottom anode and a top cathode consisting of a thin Ag layer covered with an organic capping layer. With the NPSL embedded between the substrate and the ITO layer, the proposed TL/BD-OLEDs exhibit a significantly enhanced EQE for both top emission (2.1-fold enhancement) and bottom emission (1.5-fold enhancement) with respect to the reference device. In addition, as a result of the averaging effect of the NPSL, the change in chromaticity and luminance with viewing angle is strongly reduced compared to the reference device. Simulations performed for various particle concentrations reveal that the bottom-side emission is governed by a competition between waveguide-mode extraction and backward scattering/reflection, while the top-side emission is primarily dominated by the latter. Given its simplicity and effectiveness, we believe that the proposed NPSL-based scheme can expedite the commercialization of TL/BD-OLEDs.

Acknowledgements. This work is supported by the German BMBF (13N11060, project R2FLEX) and the National Science Council and Ministry of Education of Republic of China (Taiwan) (NSC-99-2221-E-002-118-MY3 and 10R70607). H.-W. Chang acknowledges the support from Deutscher Akademischer Austauschdienst (DAAD)/NSC foundation, and he also appreciates the assistance from Dr. Tae Hyun Gil and Sebastian Franke (Fraunhofer COMEDD). J. Lee acknowledges the Alexander von Humboldt Foundation and the IT R&D program of MKE/KEIT (Grant No. 10041416, the core technology development of light- and space-adaptable new mode display for energy savings at 7 inches and 2 W). S. Yoo is supported by a National Research Foundation of Korea grant funded by the Korean government (NRF-2011-013-D00046).

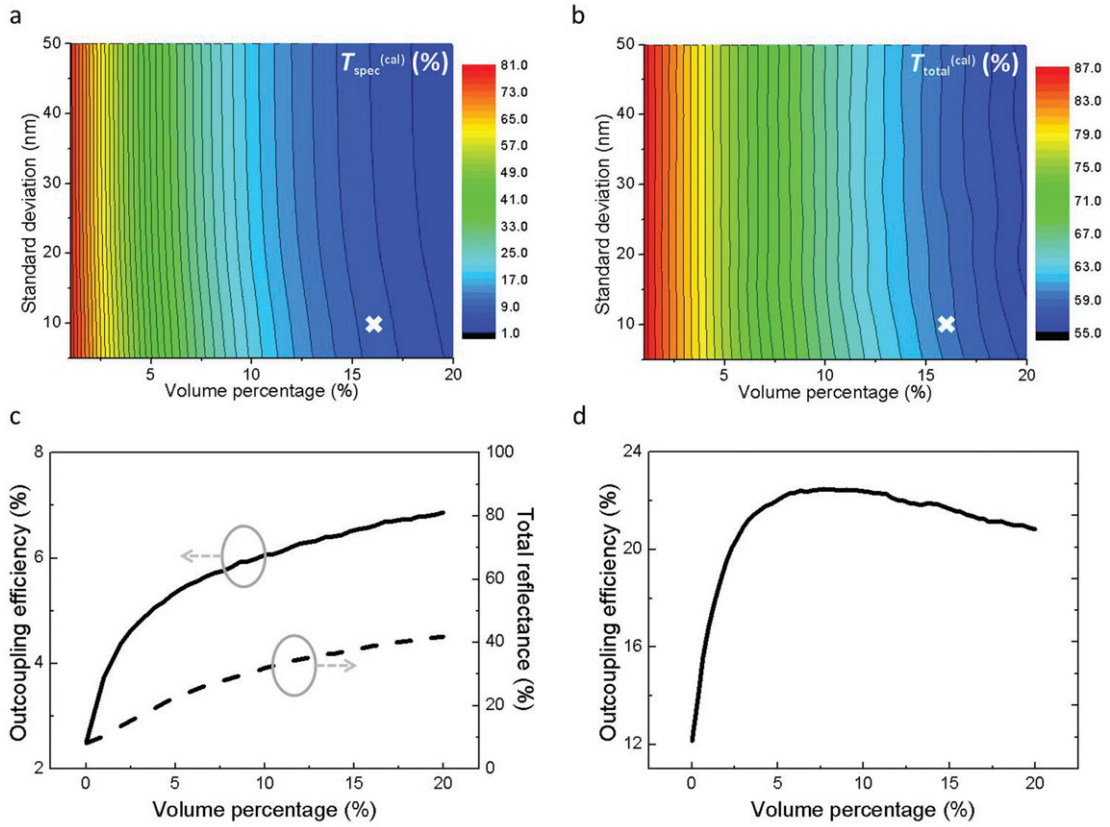

Figure 8 LightTools™ simulation results for the NPSL. a) Calculated specular transmittance of the NPSL and b) calculated total transmittance of the NPSL as a function of the particle size distribution (standard deviation of Gaussian distribution) and the volume percentage of scattering particles in the film. c) Calculated outcoupling efficiency at the top and d) bottom of the bi-directional OLED versus the volume percentage of the scattering particles. Calculated total reflectance from the NPSL is also shown in c.

Received: 1 August 2013, **Revised:** 10 September 2013, **Accepted:** 10 September 2013

Published online: 8 October 2013

Key words: bi-directional organic light emitting diodes, nanoparticle scattering layer, outcoupling enhancement.

References

[1] V. Bulovic, G. Gu, P. E. Burrows, S. R. Forrest, and M. E. Thompson, Nature **380**, 29 (1996).
[2] G. Gu, V. Bulovic, P. E. Burrows, S. R. Forrest, and M. E. Thompson, Appl. Phys. Lett. **68**, 2606 (1996).
[3] G. Gu, G. Parthasarathy, P. E. Burrows, P. Tian, I. G. Hill, A. Kahn, and S. R. Forrest, J. Appl. Phys. **86**, 4067 (1999).
[4] H. Cho, J.-M. Choi, and S. Yoo, Opt. Express **19**, 1113 (2011).
[5] L. S. Hung, C. W. Tang, M. G. Mason, P. Raychaudhuri, and J. Madathil, Appl. Phys. Lett. **78**, 544 (2001).
[6] H. Riel, S. Karg, T. Beierlein, B. Ruhstaller, and W. Riess, Appl. Phys. Lett. **82**, 466 (2003).
[7] X. Gong, P. K. Iyer, D. Moses, G. C. Bazan, A. J. Heeger, and S. S. Xiao, Adv. Func. Mater. **13**, 325 (2003).
[8] C. J. Lee, R. B. Pode, J. I. Han, and D. G. Moon, Appl. Phys. Lett. **89**, 123501 (2006).
[9] R. B. Pode, C. J. Lee, D. G. Moon, and J. I. Han, Appl. Phys. Lett. **84**, 4614 (2004).
[10] S. Y. Ryu, S. J. Jo, C. S. Kim, S. H. Choi, J. H. Noh, H. K. Baik, H. S. Jeong, D. W. Han, S. Y. Song, and K. S. Lee, Appl. Phys. Lett. **91**, 093515 (2007).
[11] T.-H. Han, Y. Lee, M.-R. Choi, S.-H. Woo, S.-H. Bae, B. H. Hong, J.-H. Ahn, and T.-W. Lee, Nat. Photon. **6**, 105 (2012).
[12] S. Reineke, F. Lindner, G. Schwartz, N. Seidler, K. Walzer, B. Lussem, and K. Leo, Nature **459**, 234 (2009).
[13] Y. Sun and S. R. Forrest, Nat. Photon. **2**, 483 (2008).
[14] C. Adachi, M. A. Baldo, M. E. Thompson, and S. R. Forrest, J. Appl. Phys. **90**, 5048 (2001).
[15] S.-Y. Kim, W.-I. Jeong, C. Mayr, Y.-S. Park, K.-H. Kim, J.-H. Lee, C.-K. Moon, W. Brütting, and J.-J. Kim, Adv. Func. Mater. n/a (2013).
[16] P. Liehm, C. Murawski, M. Furno, B. Lussem, K. Leo, and M. C. Gather, Appl. Phys. Lett. **101**, 253304 (2012).
[17] H.-W. Chang, J. Lee, S. Hofmann, Y. H. Kim, L. Muller-Meskamp, B. Lussem, C.-C. Wu, K. Leo, and M. C. Gather, J. Appl. Phys. **113**, 204502 (2013).
[18] T. Nakamura, H. Fujii, N. Juni, and N. Tsutsumi, OPT REV **13**, 104 (2006).

[19] Y.-S. Tyan, Y. Rao, X. Ren, R. Kesel, T. R. Cushman, W. J. Begley, and N. Bhandari, SID Symposium Digest of Technical Papers **40**, 895 (2009).
[20] T. Yamasaki, K. Sumioka, and T. Tsutsui, Appl. Phys. Lett. **76**, 1243 (2000).
[21] C.-L. Lin, H.-W. Lin, and C.-C. Wu, Appl. Phys. Lett. **87**, 021101 (2005).
[22] A. Isphording and M. Pralle, Organic Electronics **11**, 1916 (2010).
[23] K. Neyts, Appl. Surf. Sci. **244**, 517 (2005).